INTERNATIONAL JOURNAL OF CLIMATOLOGY
Int. J. Climatol. **38**: 2230–2238 (2018)
Published online 16 November 2017 in Wiley Online Library
(wileyonlinelibrary.com) DOI: 10.1002/joc.5329

Synoptic climatology of winter daily temperature extremes in Sapporo, northern Japan

M. A. Farukh[a]* and Tomohito J. Yamada[b]

[a] *Department of Environmental Science, Bangladesh Agricultural University, Mymensingh, Bangladesh*
[b] *Department of Engineering, Hokkaido University, Sapporo, Japan*

ABSTRACT: Extreme winter daily temperature is an important parameter for determining winter precipitation. This study used a principal component analysis and *k*-means clustering to characterize the circulation patterns of extreme daily temperatures for 19 winter seasons in Sapporo, Hokkaido, Japan. Climatological anomaly maps were constructed for sea level pressure (SLP) and the 500-hPa geopotential height for the identified minimum ($Tmin_{10}$; 239 days) and maximum ($Tmax_{90}$; 236 days) daily temperature extremes. The $Tmax_{90}$ SLP anomaly pattern was the opposite (west–east orientation) of the $Tmin_{10}$ pattern. The circulation patterns that predominantly contributed to winter rainfall were derived from cyclones over the Sea of Japan via instability created by abundant heat and moisture over the ocean and a strong positive 500-hPa height anomaly over Hokkaido.

KEY WORDS Aleutian low; geopotential height; maximum daily temperature extreme; minimum daily temperature extreme; sea level pressure; Siberian high

Received 30 June 2015; Revised 27 September 2017; Accepted 29 September 2017

1. Introduction

Hokkaido is the northernmost and second largest (77 978 km^2) Japanese island, which experiences a sub-arctic climate. Sapporo, the epicentre and capital of Hokkaido, is famous for snow-based tourism, with more than 100 days of snowfall per winter. The northwesterly winter monsoon and its inter-annual variability are vital to snowfall in Hokkaido. The snowpack begins to disappear in late March–April. Melt water is an important water resource for the local population. However, the last two decades have witnessed significant reductions in the amount of snowfall and duration and extent of sea ice in the southern Sea of Okhotsk (Hirota *et al.,* 2006), including along the coast of Hokkaido (JMA, 2007). Using the Special Report on Emissions Scenarios (SRES) A1B scenario, Mizuta *et al.* (2005) predicted a reduction of 20–45 days with frost in Hokkaido by 2090.

Downscaling-based future projections have suggested a decreasing trend in snow depth in Hokkaido (Matsumura and Sato, 2011), with more warming expected during the winter than summer and during the night than day. Winter temperature in Hokkaido is driven not only by heavy ice cover but also by northeasterly winds (Honda *et al.,* 1994) while Tachibana (1995) described snowfall distribution on the Japan Sea side of Hokkaido. Chishima (1962) indicated that years with heavy (light) ice conditions in Abashiri (facing the Sea of Okhotsk; 44°01′14″N, 144°16′24″E), Hokkaido were associated with below (above)-average temperatures. Ogara (1976) reported the relationship between winter temperature and sea ice and found that temperature dropped (rose) and sea ice approached (retreated from) the city of Abashiri, Hokkaido. Aota *et al.* (1988) described the relationship between the amount of sea ice and temperature and found a decrease in winter temperature in Monbetsu (facing the Sea of Okhotsk; 44°21′23″N, 143°21′16″E), Hokkaido. Jacobs (1946) described the distribution of the percentage of days with precipitation and air flow patterns in Hokkaido. Meanwhile, Kawamura (1961) described winter precipitation in Hokkaido considering synoptic climatological features.

Winter rainfall in Hokkaido is associated with a serious risk of landslides, mudslides, flooding, and avalanches. For example, on 21 January 2002, the Motsukisamu River near Sapporo (43°01′54″N, 141°25′00″E) was flooded (0.3 ha inundated) by a 53.5-mm rainfall event, with a maximum air temperature of 4.5 °C. Under the condition of a global 2 °C temperature increase, Yamada *et al.* (2014) estimated a 1.12-fold increase in future short-term extreme winter precipitation intensity in Hokkaido. In addition, the decline in snow cover will force changes in snow- and ice-based tourism centres, such as the ski resort town of Niseko, southwest Hokkaido (42°48′22″N, 140°41′13″E; JMA, 2007), threatening the cultural identity of Hokkaido.

Specific circulation patterns are responsible for such temperature variations in winter. Several studies have examined atmospheric circulation, with an emphasis on cyclonic activity and its influence on temperature

* Correspondence to: M. A. Farukh, Department of Environmental Science, Bangladesh Agricultural University, Mymensingh 2202, Bangladesh. E-mail: maf_bau@yahoo.com

(e.g.Przybylak, 2000 ; Zhang *et al.,* 2004 ; Rogers *et al.,* 2005). To classify these circulation patterns, principal component analysis (PCA) and clustering have been used (Birkeland *et al.,* 2001; Yarnal *et al.,* 2001; Esteban *et al.,* 2005; Bednorz, 2011; Farukh and Yamada, 2014). In this study, we identified and described the circulation patterns of sea level pressure (SLP) and 500-hPa geopotential height (G_pH) associated with maximum and minimum temperature extremes in Sapporo using a PCA and *k*-means clustering. The local effect of circulation patterns on winter snowfall and rainfall was characterized using instability indices. Section 2 introduces the methodology used in this study. The statistical characteristics and synoptic climatology of extreme temperature days are described in Section 3, and a discussion is provided in Section 4.

2. Data and methodology

This study considered the Sapporo region (42°53′38″–43°15′58″N and 141°04′52″–141°35′49″E) of the northernmost Japanese island, Hokkaido. Daily temperature data from 1992 to 2011 at 10-min intervals were obtained from the Sapporo City multi-sensor (MULTI) network, which has 52 stations (Figure 1(a)). Figure 1(b) shows the monthly variations in daily mean air temperature averaged over the 52 MULTI network stations and standard deviation (boxes), as well as the maximum and minimum daily means (whiskers) for the period of 1992–2011.

In this study, only the winter (December–March) air temperatures, rainfall, and snowfall for the 1992/1993 to 2010/2011 seasons were analysed. To characterize extreme meteorological phenomena, the maximum and minimum values are widely used as measures of dispersion and frequency of occurrence (Bednorz, 2011). In this study, based on the Intergovernmental Panel on Climate Change, the extreme daily mean temperatures were defined as those with a frequency lower (higher) than or equal to 10% (90%) (IPCC, 2007). The mean value of the 52 MULTI stations spatially averaged daily minimum temperature lower than the 10th percentile and that of the daily maximum temperature greater than the 90th percentile are referred to here as the negative (i.e. minimum; $Tmin_{10}$) and positive (i.e. maximum; $Tmax_{90}$) extremes of the mean daily temperatures, respectively.

The daily mean SLP data sets for $Tmin_{10}$ and $Tmax_{90}$ days were obtained from the Japanese 55-year reanalysis (JRA-55) by the Japan Meteorological Agency (JMA) (Kobayashi *et al.,* 2015) encompassing a region within 20°–65°N and 110°–170°E at a 1.125° spatial resolution. The daily SLP values were computed as the 6-h average (0000, 0600, 1200, and 1800 UTC) values for each day. Because a large variation remained in the daily values, Lanczos low-pass filtering (Duchon, 1979) with 121-term weighting factors and a 60-day cut-off was applied. PCA is a technique for reducing data without losing climate information, which is used extensively in meteorology and climatology (Baeriswyl and Rebetez, 1997). In this study, PCA based on an S-mode (grid points as variables, days as observations) data matrix was applied. S-mode PCA is a proven technique for climate regionalization (Knapp *et al.,* 2002), where the eigenvalues and eigenvectors of the correlation or covariance matrix of the time series and loading matrix are computed first. The PCA can be defined from an $N \times n$ data matrix $Z = (z_{ij}: i = 1,..., N; j = 1,..., n)$, where i indexes individuals or cases and j indexes variables. For every, i, j, z_{ij} denotes the variable value of a physical field or derived field. Thus, the PCA representation of z_{ij} is as follows:

$$z_{ij} = \sum_{m=1}^{r} f_{im} a_{mj}^{T} \quad i = 1, \ldots, N; \quad j = 1, \ldots, n; \quad m = 1, \ldots, r; \quad r \leq n \tag{1}$$

where f_{im} is the rth principal component (PC) score for the ith individual and a_{mj} is the rth PC loading on the jth variable.

In matrix form, Equation (1) becomes:

$$Z = FA^{T} \tag{2}$$

The PC scores or amplitudes and loadings can be developed with the following definitions:

$$R \equiv Z^{T} Z \, (n \times n) \quad \text{(data correlation matrix)} \tag{3}$$

$$\Phi \equiv F^{T} F \quad (r \times r) \quad \text{(PC score correlation matrix)} \tag{4}$$

$$S \equiv Z^{T} F \, (n \times r) \quad \text{(PC primary structure matrix)} \tag{5}$$

In Equation (5), Z^T can be substituted by AF^T,

$$Z^{T} F = A F^{T} F \tag{6}$$

$$S = A\Phi \tag{7}$$

which is a solution of the PC primary structure matrix (5) that represents the correlations between the PCs and variables. Equations (3), (4), and (6) are used to define the PCA in terms of the correlation matrix (R) representation:

$$R = Z^{T} Z = A F^{T} F A^{T}$$

$$R = A \Phi A^{T} \tag{8}$$

This relationship (Equation (8)) is the fundamental PC equation in terms of the correlation matrix and is a combination of A (PC primary pattern matrix) and $A\Phi$ (PC primary structure matrix). In the orthogonal rotation, $\Phi = I_r$; therefore, $A\Phi = A$, and both are referred to as PC loadings.

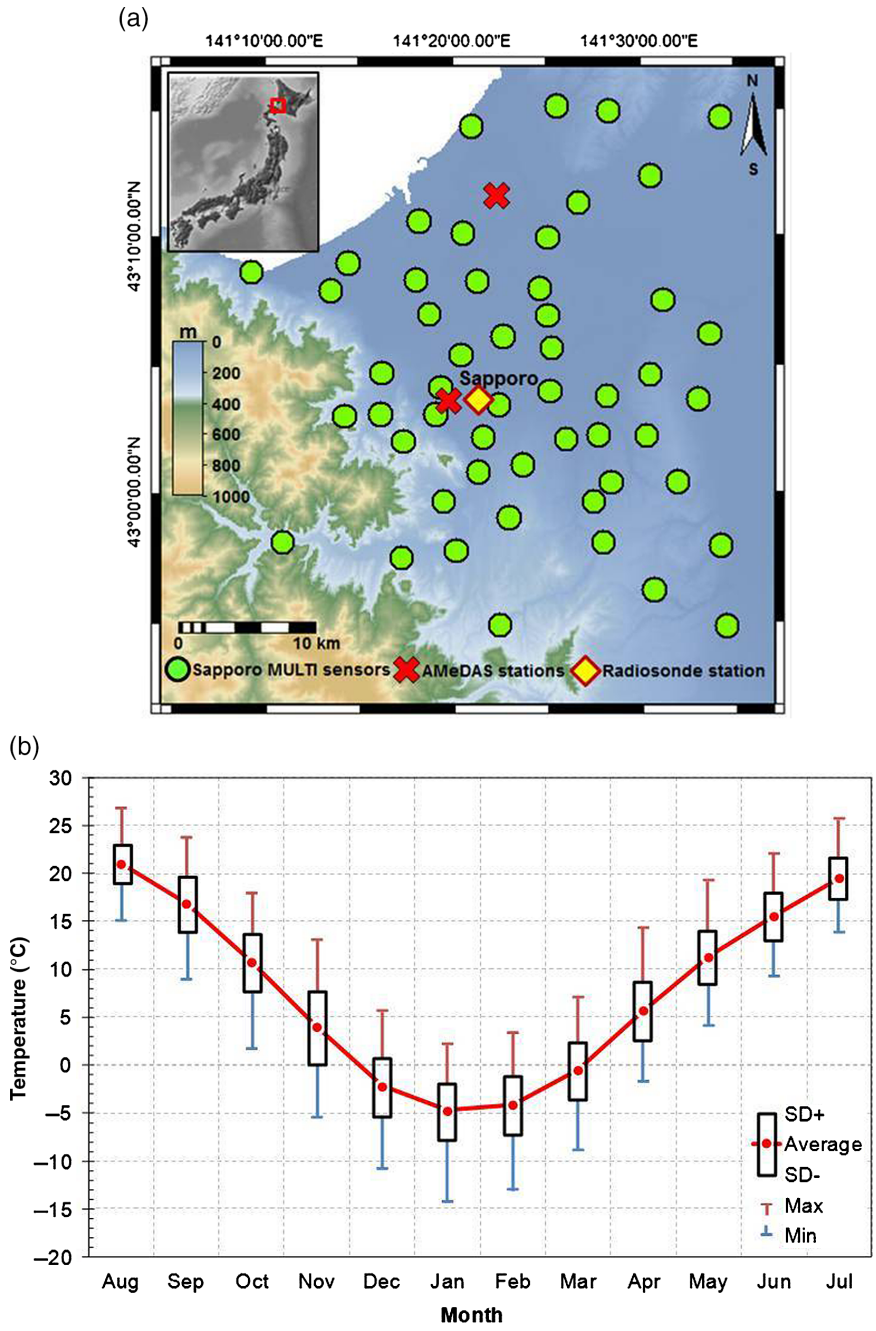

Figure 1. (a) Location of Sapporo MULTI network (52), AMeDAS (2), and radiosonde (1) stations. (b) Boxplot graph for the monthly course of air temperatures with standard deviation (box) and maximum/minimum daily means (whiskers) for the period 1992–2011 from Sapporo MULTI data set. [Colour figure can be viewed at wileyonlinelibrary.com].

The PCA was conducted on the standardized SLP (Yarnal *et al.,* 2001) to derive the dominant patterns of variability from the raw fields. Until this step of the analysis, the JRA-55 data were used to ensure the maximum precision of SLP data surrounding Japan. However, the loading matrix represents the correlation of the original variables with the PCs. The loading matrix (C) can be calculated using the following equation:

$$C = A \times \lambda^{1/2} \tag{9}$$

where A is an orthogonal matrix of the eigenvector of the correlation matrix R and λ is the diagonal matrix of eigenvalues of R. Following Barry and Carleton (2001), the correlation matrix was used to efficiently represent the variances in the data set, without possible domination by the grid points with the largest variances (Jolliffe, 1986). The number of components explaining a significant portion of the total variance was determined by the Scree test (Cattell, 1966) where the Scree test determines the number of factors retained in a PCA and involves plotting the eigenvalues in descending order of magnitude against their factor numbers. The transition from a steep slope to a plateau indicates the number of meaningful factors, which differs from the random error. The retained

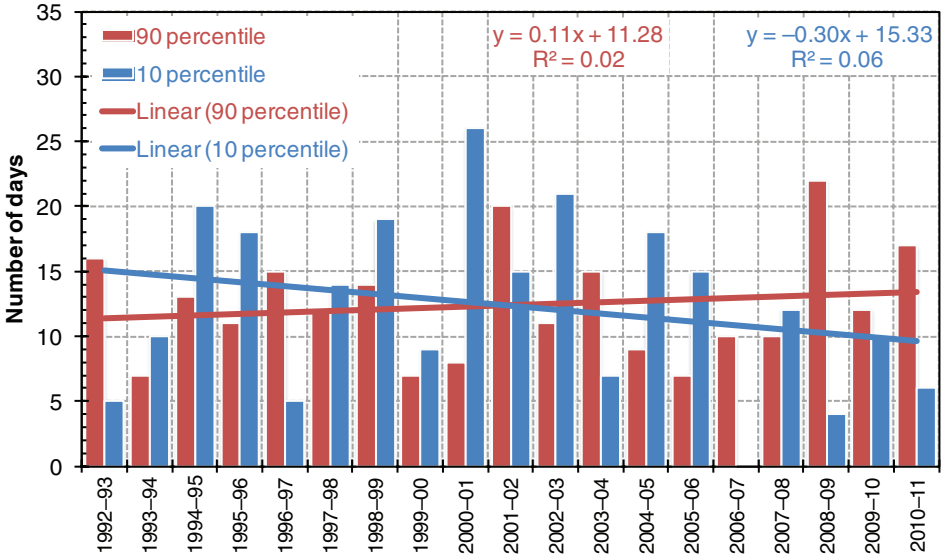

Figure 2. Multiannual values for the number of days with negative ($Tmin_{10}$) and positive ($Tmax_{90}$) winter temperature extremes with their trend lines. [Colour figure can be viewed at wileyonlinelibrary.com].

components are then rotated using a varimax procedure (Yarnal, 1993).

A non-hierarchical *k*-means clustering method, which is an objective identification technique (Yarnal, 1993; Hair *et al.,* 1998), was used to classify and cluster the observations and ensure the comparability of the results for different atmospheric data sets (e.g.Fovell and Fovell, 1993; Gerstengarbe *et al.,* 1999; Martineu *et al.,* 1999; Unal *et al.,* 2003). The clustering procedure determines the distance between individual observations using the smallest Euclidean distance. The Euclidean distance ($d_{r,s}$) is a measure of the dissimilarity between two pairs of objects (clusters) x_r and x_s, in an $n \times p$ data matrix:

$$d_{r,s} = \left[\left(x_r - x_S \right)' \left(x_r - x_S \right) \right]^{1/2} \qquad (10)$$

where n is the number of observations and p is the number of variables. To decide the number of groups and centroids, we considered the spatial variation patterns established by the PCA (i.e. the PCs in the positive and negative phases) as potential groups. To create the centroids of the groups, observations with high score values were selected ($>+1$ for the positive phase, or <-1 for the negative phase, but between $+1$ and -1 for the remainder of the PCs) (Tait and Fitzharris, 1998; Birkeland *et al.,* 2001). The *k*-means clustering also produced the final classification of all observations (days) with a similar distribution of SLP fields. Because the centroids of the classified SLP fields were well established by the first PCA grouping (reflecting a circulation pattern), non-iteration (i.e. no repetition) of the *k*-means clustering was used.

Finally, synoptic maps of the circulation groups were constructed for SLP and G_pH. To derive the synoptic circulation patterns, daily SLP and G_pH data were used from the National Centers for Environmental Prediction/National Center for Atmosphere Research (NCEP/NCAR) reanalysis (Kalnay *et al.,* 1996), which ensured quality atmospheric data at a 2.5° grid resolution. The SLP and G_pH climatological anomaly maps were constructed separately for $Tmin_{10}$ and $Tmax_{90}$. The MULTI rainfall and snowfall data for the individual circulation groups were compared with data from the Automated Meteorological Data Acquisition System (AMeDAS; Figure 1(a)), which is maintained by the JMA. The radiosonde data for the days of $Tmin_{10}$ and $Tmax_{90}$ for the Sapporo stations measured at 0900 JST (UTC+9) were derived from the web portal of the Department of Atmospheric Science, University of Wyoming.

3. Results

3.1. Extreme temperature days

A total of 239 days with $Tmin_{10}$ and 236 days with $Tmax_{90}$ were selected from 19 winter seasons for further analysis. The threshold values determined for $Tmin_{10}$ and $Tmax_{90}$ were ≤ -19.85 and ≥ 10.22 °C, respectively. On a multi-annual scale, the number of days with extreme temperatures displayed considerable year-to-year variability (Figure 2). The number of days with $Tmin_{10}$ showed a decreasing trend, and the mean winter temperature in Sapporo, which was derived from the spatially averaged December–March temperature at 52 MULTI stations, rose by 0.5 °C over the last two decades. The PCA and SLP clustering for $Tmin_{10}$ and $Tmax_{90}$ enabled the selection of five PCs for each set of extremes, which explained 82 and 81% of the total variance, respectively.

Finally, $Tmin_{10}$ and $Tmax_{90}$ days were classified into five groups for each set of extremes. The winter mean SLP showed the development of two main centres, the Siberian high over the Eurasian continent (centre pressure: ~1030 hPa) and the Aleutian low over the North Pacific (centre pressure: ~996 hPa). Hokkaido is located between the perimeters of these two systems (Figure 3(a)), where

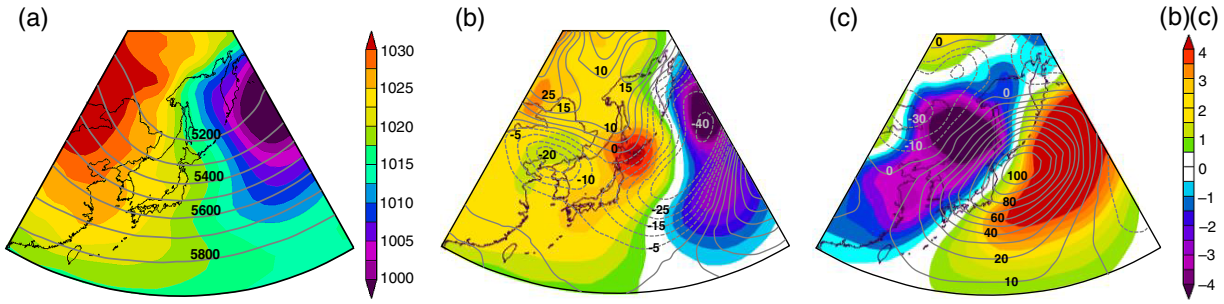

Figure 3. (a) Seasonal mean SLP in hPa (shading) and 500 hPa height in meter (solid lines) for the winter season (December–March: 1992–2011). (b) SLP (hPa) and 500 hPa height (m) of the $Tmin_{10}$ composite anomaly from climatology (DJFM: 1981–2010). (c) Same as (b) but for $Tmax_{90}$. [Colour figure can be viewed at wileyonlinelibrary.com].

the prevailing northwesterly winds cause the advection of a cold air mass from Siberia and abundant moisture from the Sea of Japan to Hokkaido that can cause heavy snowfall in western Hokkaido. Conversely, the mean G_pH increased from the south of Japan (5800 gpm) to the north (<5300 gpm over Hokkaido).

3.2. Synoptic climatology of $Tmin_{10}$

The SLP composite for $Tmin_{10}$ showed a strong (>4 hPa) positive anomaly surrounding Hokkaido, with a centre held to the east by the Aleutian low (Figure 3(b)). Conversely, the positive G_pH anomaly extended over northern Hokkaido, suggestive of a predominantly northwesterly airflow in the mid-troposphere. The transition zone between the positive and negative anomaly covered the entirety of Hokkaido. The clustering of $Tmin_{10}$ revealed the five most relevant types (clusters 1–5); their anomalies relative to climatology are shown in Figure 4(a) (shading). Clusters 1–5 represented 60, 57, 14, 26, and 82 days, respectively. In addition, 52% of days in cluster 5 appeared in January, which had the maximum average snowfall intensity (i.e. snow depth) of 2.4 mm h^{-1}. All clusters (except 4) showed a positive SLP anomaly over Hokkaido, but they differed in terms of location and pressure centre intensity. The maximum positive anomaly (>5 hPa) was found over eastern Hokkaido (cluster 2), while the cyclonic systems or disturbances were located over the west of Bering Sea (clusters 1, 4, and 5). The western high was a strong feature (cluster 4) that could form a narrow ridge over Hokkaido and spread up to the west of Bering Sea, causing very intense airflow from the north/northwest. This circulation type (particularly the Siberian high) in the cold season consisted of a cold dry air mass that could carry cold outbreaks toward the East Asian region (Wang, 2006), with a prominent effect on northern Japan. Cluster 3 showed a different pattern, with the strongest positive anomaly (>7 hPa) over the west of Bering Sea and a cyclone over southern Japan, which could bring heavy snowfall to the Pacific coast of Honshu. Figure 4(a) also illustrates the G_pH anomaly (solid and dotted lines for positive and negative anomalies, respectively), where clusters 4 and 5 were characterized by a strong negative anomaly (−20 to −50 gpm) over Hokkaido from the west of Bering Sea. Conversely, a positive anomaly dominated over Hokkaido, originating from the west of Bering Sea (clusters 2 and 3, partly positive for cluster 1).

3.3. Synoptic climatology of $Tmax_{90}$

Figure 3(c) shows the negative SLP anomaly (<−3 hPa) over Hokkaido, with a centre over the Eurasian continent, while a strong G_pH (100 gpm) positive anomaly existed over southeast Hokkaido. Regarding $Tmax_{90}$, clusters 1–5 represented 32, 14, 60, 44, and 86 days, respectively. Moreover, 56% days in cluster 5 were observed in March, which had the maximum average rainfall of 4.17 mm day^{-1}.

Figure 4(b) shows the circulation types (clusters 1–5) and their SLP (shading) and G_pH (lines) anomalies for $Tmax_{90}$, which showed a strong (<−7 hPa) negative SLP anomaly (clusters 1, 2, 4, and 5) from the west/northwest of Hokkaido, while a strong (>7 hPa) positive zone existed over the west of Bering Sea except cluster 4. The main feature of these circulation types was a low-pressure trough extending over Hokkaido and a cyclone over the Sea of Japan. On the side of Hokkaido adjacent to the Sea of Japan, the synoptic patterns shown in Figure 4(b) correspond to southerly (warm) wind rather than the winter monsoon. In most of these cases, seasonal precipitation led by the winter monsoon absorbed latent heat from the Sea of Japan (Hirose and Fukudome, 2006), which was responsible for extreme rainfall events in Hokkaido (Figure 6), categorized as Dfa or Dfb in the Köppen–Geiger climate classification (Peel *et al.,* 2007). Conversely, winter rainfall in the area of Hokkaido adjacent to the Pacific Ocean was carried by extra-tropical cyclones passing across Japan or passing near the southeastern coastal areas. This type of rainfall becomes active in early winter in Hokkaido due to active cyclogenesis. A positive anomaly inflow from the north was apparent for the least common circulation type (cluster 3). The G_pH indicated a positive anomaly over Hokkaido for all clusters, when the strongest (>50 gpm; clusters 4 and 5) had very steep contour gradients suggestive of a mostly westerly/southwesterly airflow, but for cluster 2 the 500 hPa wind over Hokkaido was from the southeast.

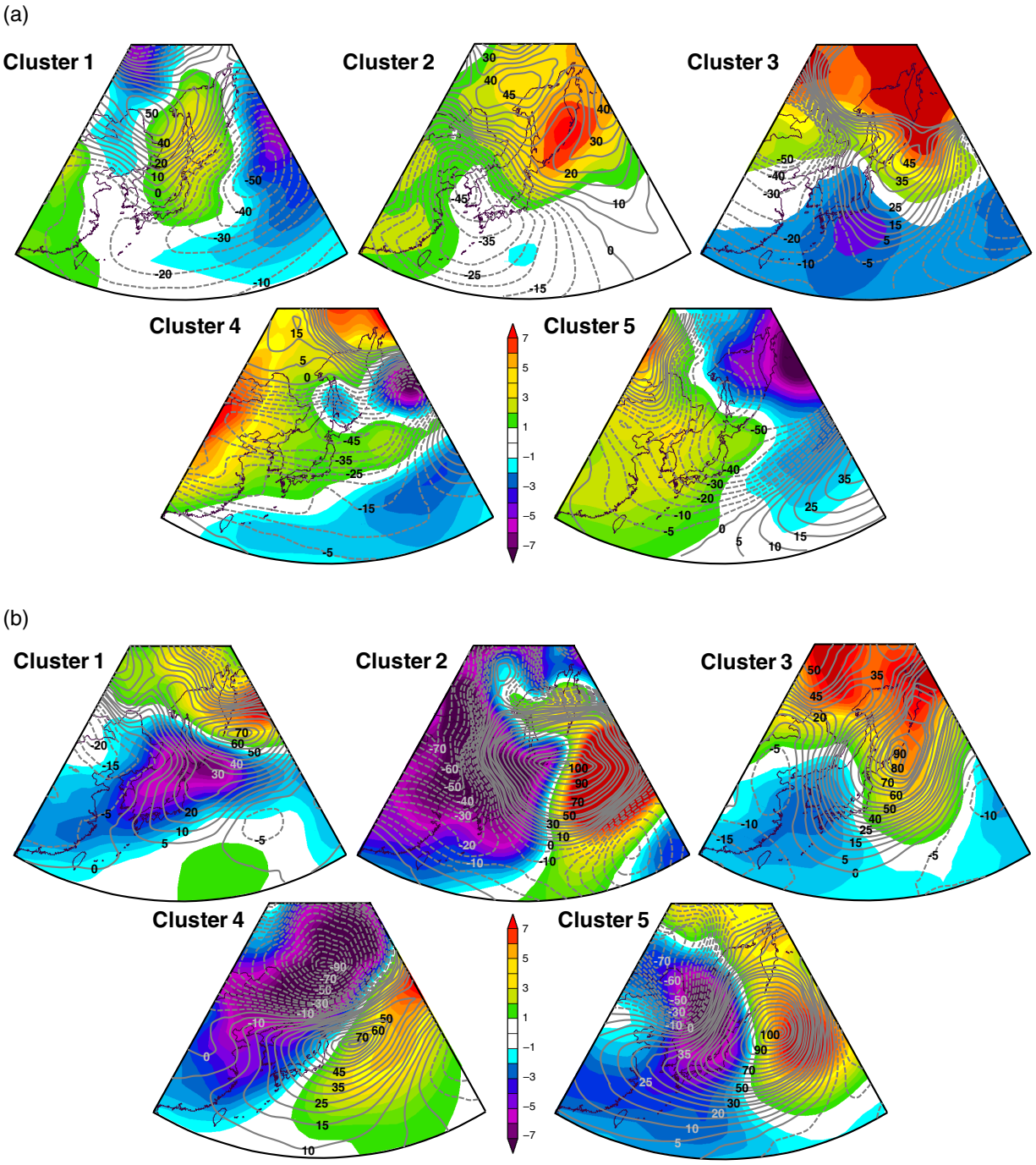

Figure 4. (a) SLP in hPa (shading) and 500 hPa height in meter [lines: solid (positive anomaly) and dotted (negative anomaly)] anomaly for the classified five groups for the days with minimum temperature extremes ($Tmin_{10}$). (b) SLP in hPa (shading) and 500 hPa height in meter [lines: solid (positive anomaly) and dotted (negative anomaly)] anomaly for the classified five groups for the days with maximum temperature extremes ($Tmax_{90}$). [Colour figure can be viewed at wileyonlinelibrary.com].

3.4. Characteristics of $Tmin_{10}$ and $Tmax_{90}$

To characterize extreme temperature days, the contribution of circulation patterns was evaluated based on snowfall (for $Tmin_{10}$) and rainfall (for $Tmax_{90}$) (Figures 5(a) and (c)), along with sunshine hours (from MULTI) and upper air instability indices (from the University of Wyoming), such as convective available potential energy (CAPE), convective inhibition (CIN), and precipitable water (PWAT) (Figures 5(b) and (d)). The graphical representation of the variability or the uncertainties of the measurements for all parameters are shown using vertical bars. In addition, Figure 6 shows the spatial distribution of rainfall and snowfall over Hokkaido for each cluster type using AMeDAS data for $Tmax_{90}$ (first and third panels) and $Tmin_{10}$ (second and fourth panels). The separation of AMeDAS precipitation into 10-km gridded rainfall and snowfall intensity was applied by the threshold of 2 °C at 2-m-height air temperature.

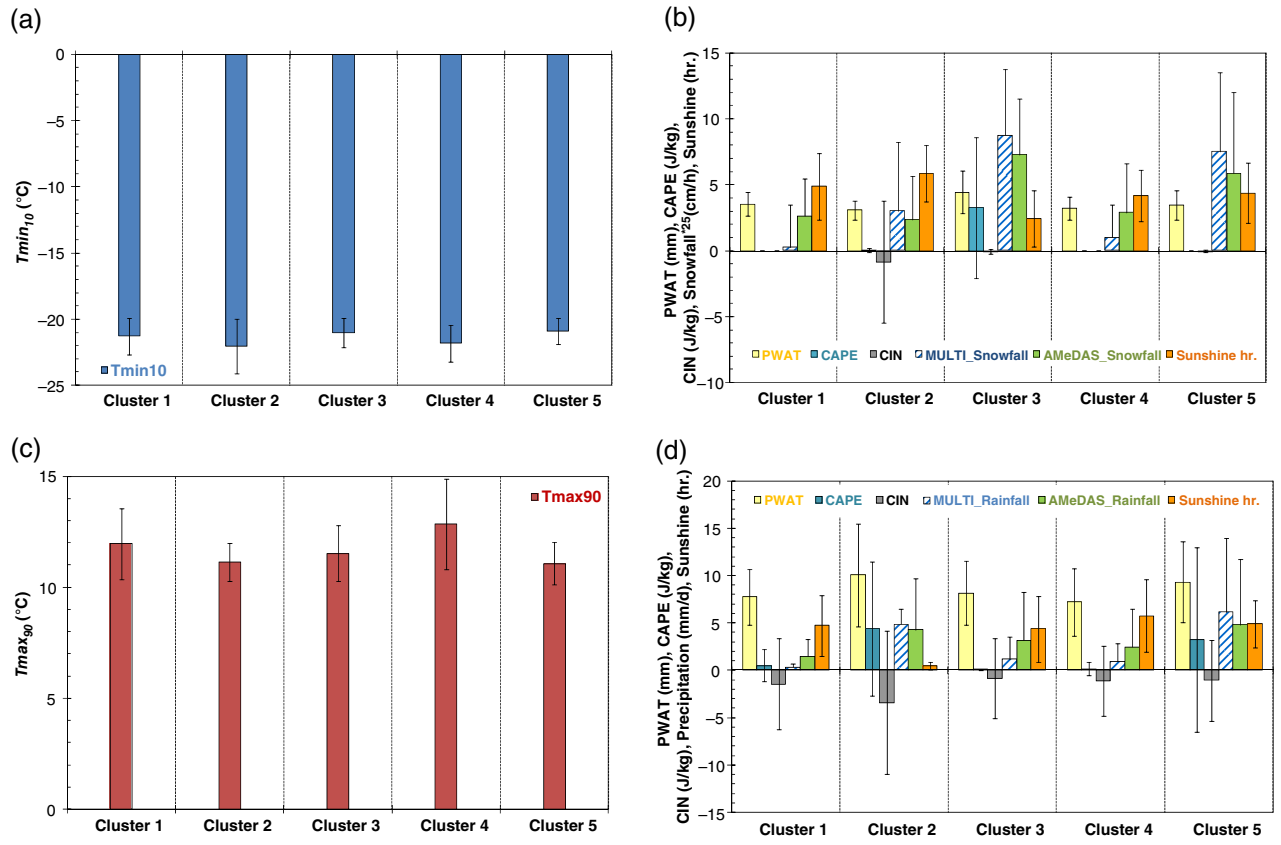

Figure 5. (a) Minimum temperature extremes ($Tmin_{10}$) and (b) PWAT, CAPE, CIN, snowfall (MULTI and AMeDAS), and sunshine hour for all the identified clusters. (c), (d) Same figures but for maximum temperature extremes ($Tmax_{90}$). [Colour figure can be viewed at wileyonlinelibrary.com].

Of the 239 days of $Tmin_{10}$, 206 days had $\geq$10 cm day^{-1} snowfall in Sapporo based on AMeDAS daily data measurements (*y*-axis in Figure 5(b); snowfall is divided by 25). Clusters 5, 3, and 2 (Figure 4(a)) accounted for 51, 27, and 13% of these snowfall days, although cluster 5 was characterized by sunny weather ($\sim$4 h day^{-1}). Although the number of sunshine hours was lower for cluster 3, it had a higher CAPE value than the other clusters, suggestive of an unstable atmosphere. On average, 3.5, 5.2, 4.6, and 2 days month^{-1} from December to March had $\geq$10 cm day^{-1} snowfall; the top three values were 24 (2004–2005), 20 (1994–1995), and 19 (1993–1994, 1998–1999, 1999–2000, and 2005–2006).

Of the 236 days of $Tmax_{90}$, 193 days had $\geq$10 mm day^{-1} of rainfall in Sapporo. Clusters 1–5 accounted for 8, 25, 17, 8, and 42% of these days. The top three numbers of days in a season were 21 (1993–1994), 20 (2004–2005), and 16 (1998–1999 and 2003–2004), while the number of rainfall days/month in December to March averaged 3.75, 3.5, 2.75, and 2.15 days, respectively. The maximum wintertime rainfall was recorded in clusters 5 and 2, where the circulation patterns were characterized by upper air instability (higher CAPE and CIN) and higher PWAT. Because of the added heat and moisture supplied by the warm ocean, as the continental air mass proceeded eastward over the Sea of Japan (Figure 4(b), clusters 2, 4, and 5), the vertical temperature profile became unstable, which caused rapid air mass transformation with abundant moisture over the Sea of Japan. Therefore, the predominantly westerly wind was forced to ascend along the mountain range of northern Japan, causing heavy rainfall, mainly on the Sea of Japan side. Although cluster 5 had a higher number of sunshine hours, the minimum number of sunshine hours with a high CAPE for cluster 2 indicated that cloudy and stormy weather was mainly governed by cyclones.

4. Discussion and conclusions

In Sapporo, northern Japan, extreme winter temperatures are important parameters for determining winter rainfall and snowfall; therefore, the drivers of temperature extremes should be investigated thoroughly. Circulation patterns at the surface and mid-troposphere have a major impact on the occurrence of temperature extremes. We used multi-variate statistics (PCA and clustering) to interpret the circulation patterns and describe extreme temperature days for 19 winter seasons (1992/1993 to 2010/2011) in Sapporo, during which time a total of 239 and 236 days were identified as $Tmin_{10}$ and $Tmax_{90}$, respectively. The frequency of $Tmin_{10}$ appears to have decreased in the last two decades. $Tmax_{90}$ displayed a slight positive trend. Using simple thresholds for snowfall ($\geq$10 cm day^{-1}) and rainfall ($\geq$10 mm day^{-1}), the total number of days with $Tmin_{10}$ ranged from 4 (2008–2009) to 26 (2000–2001) and for $Tmax_{90}$ the range was

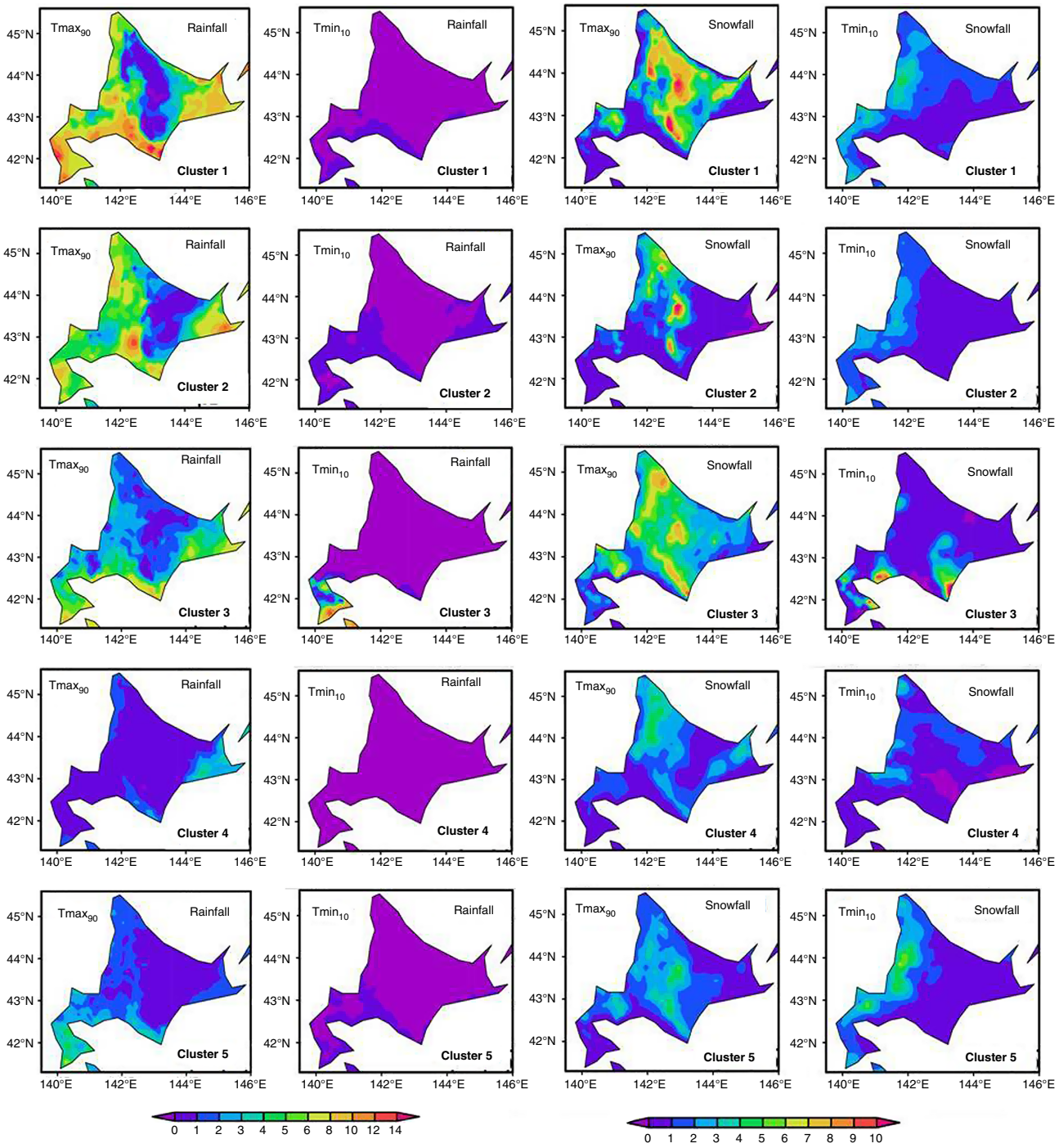

Figure 6. Spatial map of rainfall (mm day^{-1}) and snowfall (mm day^{-1}) distribution all over Hokkaido for each cluster type using AMeDAS data for maximum ($Tmax_{90}$; first and third panel) and minimum temperature extremes ($Tmin_{10}$; second and fourth panel). [Colour figure can be viewed at wileyonlinelibrary.com].

from 7 (1993–1994, 1999–2000, and 2005–2006) to 22 (2008–2009), respectively. The monthly average maximum number of days was 5.2 (January) and 3.75 (December) for $Tmin_{10}$ and $Tmax_{90}$, respectively.

Regarding $Tmin_{10}$, the pressure gradient between the Eurasian continent and northwestern Pacific (Figure 4(a); clusters 1, 3, 4, and 5) is one of the driving forces that can cause intense airflow from the north/northwest over Hokkaido. The air mass transformation process over the Sea of Japan and the ocean's role in modulating winter snowfall over northern Japan are also important regulatory factors of $Tmin_{10}$. The circulation patterns corresponding to clusters 3 and 5 (Figure 4(a)) contributed the maximum number of days within $Tmin_{10}$ (78%), which were associated with substantial snowfalls during the winter seasons included in this study.

In terms of west–east high- and low-pressure orientation, the pattern of SLP anomalies for $Tmax_{90}$ was the opposite of the pattern for $Tmin_{10}$. A rapid temperature increase associated with the passage of a cyclone can cause

heavy winter rainfall in northern Japan and is a driving force of $Tmax_{90}$. Circulation patterns are another driving force, where the location and intensity of winter cyclones (over the Sea of Japan), along with a strong positive G_pH anomaly over Hokkaido, contribute greatly to winter rainfall (Figure 4(b); cluster 2). Cluster 2 accounted for 25% of the total winter rainfall days with $\geq 10\,mm\,day^{-1}$, whereas cluster 5 accounted for the largest (42%) number of total rainfall days under an unstable atmosphere, and was strongly controlled by air circulation, particularly cyclonic activity.

Acknowledgements

The authors are thankful to Sapporo City Office, Hokkaido providing reliable data sets of Sapporo MULTI sensors. This study was partially supported by MEXT/SI-CAT and MEXT/ArCS, the CREST/JST, and JSPS KAKENHI Grant Number 17H0331837 and 15H0226707.

References

Aota M, Ishikawa M, Uematsu E. 1988. Variation in ice concentration of Hokkaido Island. *Low Temp. Sci. A: Phys.* **39**: 161–175 (in Japanese with English abstract).

Baeriswyl PA, Rebetez M. 1997. Regionalization of precipitation in Switzerland by means of principal component analysis. *Theor. Appl. Climatol.* **58**: 31–41.

Barry RG, Carleton AM. 2001. *Synoptic and Dynamic Climatology*. Routledge: London.

Bednorz E. 2011. Occurrence of winter air temperature extremes in central Spitsbergen. *Theor. Appl. Climatol.* **106**: 547–556. https://doi.org/10.1007/s00704-011-0423-y.

Birkeland KW, Mock CJ, Shinker JJ. 2001. Avalanche extremes and atmospheric circulation patterns. *Ann. Glaciol.* **32**: 135–140. https://doi.org/10.3189/172756401781819030.

Cattell RB. 1966. The Scree test for the number of factors. *Multivar. Behav. Res.* **1**: 245–276.

Chishima S. 1962. On the sea ice off Abashiri. *J. Meteorol. Res.* **14**: 639–673.

Duchon CE. 1979. Lanczos filtering in one and two dimensions. *J. Appl. Meteorol.* **18**: 1016–1022.

Esteban P, Jones P, Martin J, Mases M. 2005. Atmospheric circulation patterns related to heavy snowfall days in Andorra, Pyrenees. *Int. J. Climatol.* **25**: 319–329. https://doi.org/10.1002/joc.1103.

Farukh MA, Yamada TJ. 2014. Synoptic climatology associated with extreme snowfall events in Sapporo city of northern Japan. *Atmos. Sci. Lett.* **15**: 259–265. https://doi.org/10.1002/asl2.497.

Fovell RG, Fovell MY. 1993. Climate zones of the conterminous United States defined using cluster analysis. *J. Clim.* **11**: 2103–2135.

Gerstengarbe FW, Werner PC, Fraedrich K. 1999. Applying non-hierarchical cluster analysis algorithms to climate classification: some problems and their solution. *Theor. Appl. Climatol.* **3**(4): 143–150.

Hair JF, Anderson RE, Tatham RL, Black WC. 1998. *Multivariate Data Analysis*, 5th edn. Prentice-Hall International: Jersey City, NJ.

Hirose N, Fukudome K. 2006. Monitoring the Tsushima warm current improves seasonal prediction of the regional snowfall. *SOLA* **2**: 61–63. https://doi.org/10.2151/sola.2006-016.

Hirota T, Iwata Y, Hayashi M, Suzuki S, Hamasaki T, Sameshima R, Takayabu I. 2006. Decreasing soil-frost depth and its relation to climate change in Tokachi, Hokkaido, Japan. *J. Meteorol. Soc. Jpn.* **84**: 821–833. https://doi.org/10.2151/jmsj.84.821.

Honda M, Tachibana Y, Wakatsuchi M. 1994. The influences of the sea ice and the wind field on the winter air temperature variation in Hokkaido. *Polar Meteorol. Glaciol.* **8**: 81–94.

IPCC. 2007. Global climate projections. In *Climate Change 2007: The Physical Science Basis. Contribution of Working Group I to the Fourth Assessment Report*. Cambridge University Press: Cambridge, UK.

Jacobs WC. 1946. Synoptic climatology. *Bull. Am. Meteorol. Soc.* **27**: 306–311.

JMA. 2007. Climate change monitoring report 2006. JMA, Tokyo, 93 pp. http://ds.data.jma.go.jp/tcc/tcc/products/gwp/CCMR2006.pdf (accessed 13 March 2008).

Jolliffe IT. 1986. *Principal Component Analysis*. Springer: New York, NY.

Kalnay E, Kanamitsu M, Kistler R, Collins W, Deaven D, Gandin L, Iredell M, Saha S, White G, Woollen J, Zhu Y, Leetmaa A, Reynolds R, Chelliah M, Ebisuzaki W, Higgins W, Janowiak J, Mo KC, Ropelewski C, Wang J, Jenne R, Joseph D. 1996. The NCEP/NCAR 40-year reanalysis project. *Bull. Am. Meteorol. Soc.* **77**: 437–471.

Kawamura T. 1961. The synoptic climatological consideration on the winter precipitation in Hokkaido. *Geogr. Rev. Jpn.* **34**: 583–595 (in Japanese with English abstract). https://doi.org/10.4157/grj.34.583.

Knapp PA, Grissino-Mayer HD, Soule PT. 2002. Climate regionalization and the spatio-temporal occurrence of extreme single-year drought events (1500–1998) in the interior Pacific Northwest, USA. *Quat. Res.* **58**: 226–233.

Kobayashi S, Ota Y, Harada Y, Ebita A, Moriya M, Onoda H, Onogi K, Kamahori H, Kobayashi C, Endo H, Miyaoka K, Takahashi K. 2015. The JRA-55 reanalysis: general specifications and basic characteristics. *J. Meteorol. Soc. Jpn.* **93**: 5–48. https://doi.org/10.2151/jmsj.2015-001.

Martineu C, Caneill JY, Sadourny R. 1999. Potential predictability of European winters from the analysis of seasonal simulations with an AGCM. *J. Clim.* **12**: 3033–3061.

Matsumura S, Sato T. 2011. Snow/ice and cloud responses to future climate change around Hokkaido. *SOLA* **7**: 205–208. https://doi.org/10.2151/sola.2011-052.

Mizuta R, Uchiyama T, Kamiguchi K, Kitoh A, Noda A. 2005. Changes in extremes indices over Japan due to global warming projected by a global 20-km-mesh atmospheric model. *Sci. Online Lett. Atmos.* **1**: 153–156. https://doi.org/10.2151/sola 2005-040.

Ogara T. 1976. On the relationship between the sea ice generation and meteorological and marine phenomena in the Okhotsk sea (I), (II). *Sea Sky* **51**: 121–141.

Peel MC, Finlayson BL, McMahon TA. 2007. Updated world map of the Köppen–Geiger climate classification. *Hydrol. Earth Syst. Sci.* **11**: 1633–1644. https://doi.org/10.5194/hess11-1633-2007.

Przybylak R. 2000. Temporal and spatial variation of surface air temperature over the period of instrumental observations in the Arctic. *Int. J. Climatol.* **20**: 587–614. https://doi.org/10.1002/(SICI)1097-0088(200005)20:6<587::AID-JOC480>3.0.CO;2-H.

Rogers JC, Yang L, Li L. 2005. The role of Fram Strait winter cyclones on sea ice flux and on Spitsbergen air temperatures. *Geophys. Res. Lett.* **32**: L06709. https://doi.org/10.1029/2004GL022262.

Tachibana Y. 1995. A statistical study of the snowfall distribution on the Japan sea side of Hokkaido and its relation to synoptic-scale and meso-scale environments. *J. Meteorol. Soc. Jpn.* **73**: 697–715.

Tait AB, Fitzharris BB. 1998. Relationship between New Zealand rainfall and south-west Pacific pressure patterns. *Int. J. Climatol.* **18**: 407–424.

Unal Y, Kindap T, Karaca M. 2003. Redefining the climate zones of Turkey using cluster analysis. *Int. J. Climatol.* **23**: 1045–1055. https://doi.org/10.1002/joc.910.

Wang B. 2006. *The Asian Monsoon*. Springer Praxis Books, Praxis Publishing: Chichester, UK, 787 pp.

Yamada TJ, Farukh MA, Fukushima T, Inatsu M, Sato T, Pokhrel YN, Oki T. 2014. Extreme precipitation intensity in future climates associated with the Clausius–Clapeyron-like relationship. *Hydrol. Res. Lett.* **8**: 108–113. https://doi.org/10.3178/hrl.8.108.

Yarnal B. 1993. *Synoptic Climatology in Environmental Analysis*. Belhaven Press: London.

Yarnal B, Comrie AC, Frakes B, Brown DP. 2001. Developments and prospects in synoptic climatology. *Int. J. Climatol.* **21**: 1923–1950. https://doi.org/10.1002/joc.675.

Zhang X, Walsh JE, Zhang J, Bhatt US, Ikeda M. 2004. Climatology and inter-annual variability of Arctic cyclone activity: 1948–2002. *J. Clim.* **17**: 2300–2317. https://doi.org/10.1175/1520-0442(2004)017<2300:CAIVOA>2.0.CO;2.